

Electronic Supplementary Information (ESI)

Polymorphism-Dependent Aggregation Induced Emission of a Push-Pull Dye and its Multi-Stimuli Responsive Behavior

Chiara Botta,^{*a} Sara Benedini,^b Lucia Carlucci,^c Alessandra Forni,^{*d,e} Daniele Marinotto,^c Andrea Nitti,^b Dario Pasini,^{*b,f} Stefania Righetto^{c,e} and Elena Cariati^{*c,e}

^a ISMAC-CNR, Via Corti 12, 20133 Milano, Italy.

^b Department of Chemistry, University of Pavia, Viale Taramelli 10, 27100 Pavia, Italy.

^c Department of Chemistry, University of Milano, Via Golgi 19, 20133 Milano, Italy.

^d ISTM-CNR, Istituto di Scienze e Tecnologie Molecolari – Consiglio Nazionale delle Ricerche, via Golgi 19, 20133 Milano, Italy

^e INSTM Research Unit, University of Milano.

^f INSTM Research Unit, University of Pavia.

Experimental Details

The preparation of **1** was carried out adapting a previously published protocol. Et₃N (22 mL, 25 mmol, 3.6 equiv) in MeCN (22 mL) and then AgOCOCF₃ (642 mg, 18 mmol, 2.5 equiv) in MeCN (22 mL) were added to a solution of commercially available (Sigma Aldrich) 4,4'-bis(dimethylamino)thiobenzophenone (2 g, 7 mmol) and malononitrile (557 mg, 8 mmol, 1.2 equiv) in MeCN (22 mL). AcOEt (200 mL) and brine (200 mL) were added to the reaction suspension, which was then filtered to remove insoluble Ag₂S, and the organic and aqueous phases partitioned in a separating funnel. The organic phase was separated, dried (Na₂SO₄), and the product purified by column chromatography (SiO₂; CH₂Cl₂) to obtain an orange solid (2.1 g, 94%). *R*_f = 0.4 (CH₂Cl₂). ¹H-NMR (CDCl₃, 200 MHz, 25°C) δ = 7.41 (d, 2H; *J* = 9 Hz; ArH), 6.69 (d, 2H; *J* = 9 Hz; ArH), 3.08 (s, 12H; -N(CH₃)₂). ¹³C NMR (CDCl₃, 75 MHz, 25°C) δ = 173.8 (Cq), 153.1 (Cq), 133.5 (Cq), 123.0 (CH), 117.2 (CqCN), 110.8 (CH), 69.06 (Cq), 39.9 (-N(CH₃)₂). MS-ESI *m/z* (%) = 317 [M + H]⁺, 633 [2M + Na]⁺.

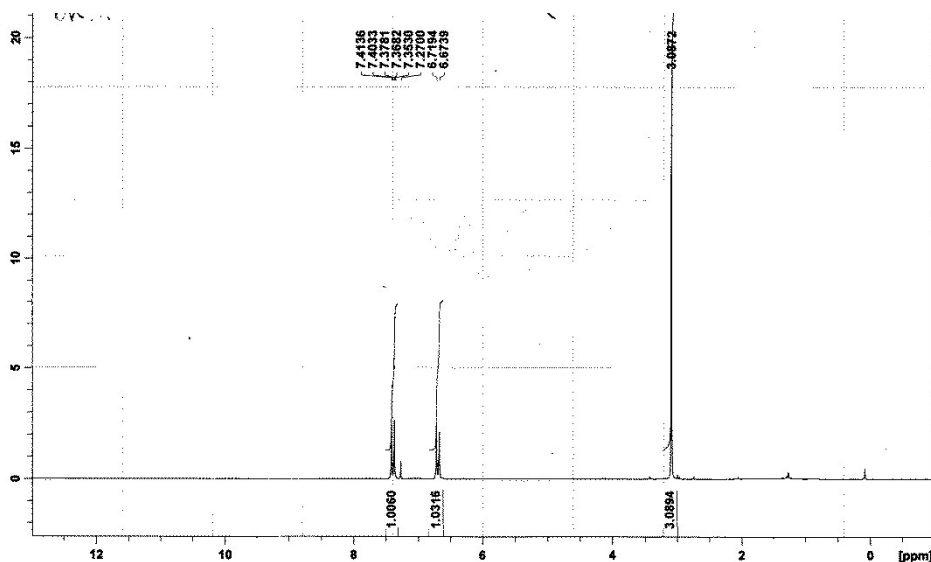


Fig. S1. ¹H-NMR spectrum (CDCl₃, 200 MHz, 25°C) of **1**.

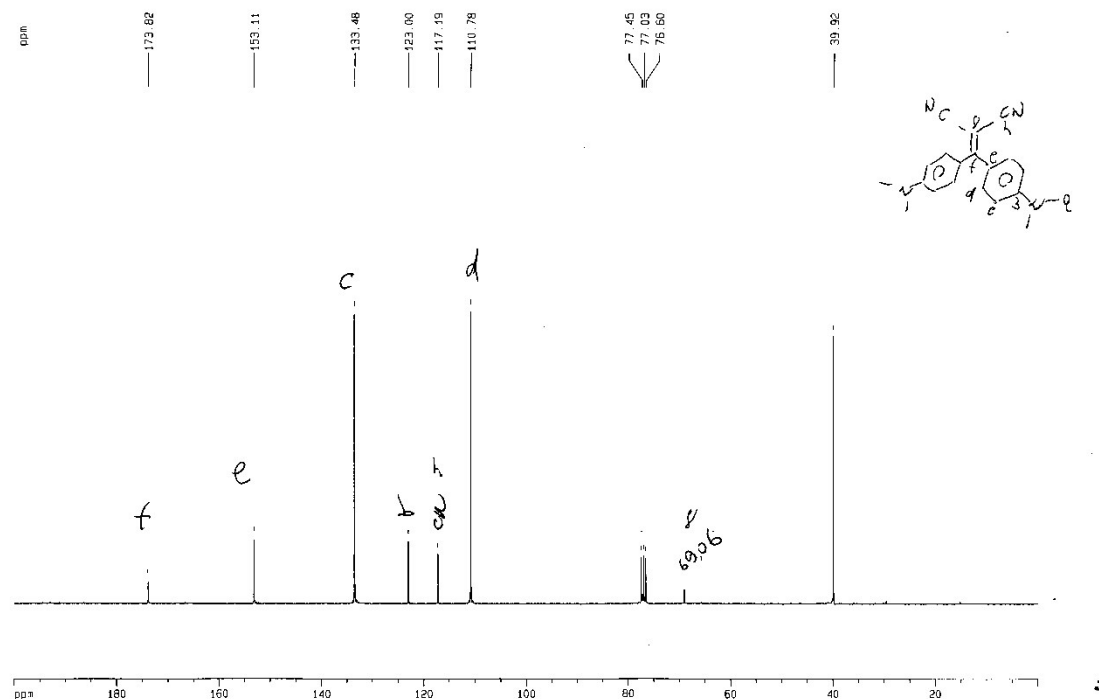


Fig. S2. ^{13}C -NMR spectrum (CDCl_3 , 75 MHz, 25°C) of **1**.

Additional Computational Details.

To investigate the electronic and optical properties of **1**, we have tested three functionals, PBE0, CAM-B3LYP and M062X. The former was used for both geometry optimization and TDDFT calculations, while the latter have been used for TDDFT calculations on the B3LYP optimized structure. In Figure S3 we plot the FMOs as obtained by the three tested approaches, while in Table S1 we report the corresponding values of selected geometrical parameters, the ground and excited states dipole moments and the low energy excitations. All functionals provided a quite similar description of the geometrical, electronic and optical properties of the molecule, with particular reference to its conjugation scheme, the FMOs distribution and the presence of two quite close excitation energies simulating the single absorption band observed in toluene at 421 nm. The only significant difference is observed in the $S_0 \rightarrow S_1$, $S_0 \rightarrow S_2$ assignments, which are swapped in CAM-B3LYP and M062X calculations with respect to those provided by PBE0 calculations. As a result, the dipole moments of the first and the second excited states, μ_{e1} and μ_{e2} , are swapped according to the used functional. The final choice of PBE0 among the tested functionals was dictated by the better agreement between the observed λ_{max} and the two computed excitation energies, which were 415 and 408 nm using PBE0, 373 and 364 nm using CAM-B3LYP, and 380 and 372 nm using M062X.

Table S1. Selected geometrical parameters, dipole moments and excitations energies (λ , nm) with associated oscillator strengths (f) and assignments based on MO contributions, computed on **1** optimized in the point group C_2 at different levels of theory in toluene.^a

Method	β	α	C=C	C-C(CN)	C-C(Ph)	$\mu_g, \mu_{e1}, \mu_{e2}$	$\lambda_{\text{abs}}(f)$, assignments
PBE0/6-311++G(d,p)	13.88	65.	1.388	1.421	1.458	13.89,	415 (0.71), H-1→L (99.2%)
//PBE0/6-311++G(d,p)		1				19.11, 16.27	408 (0.47), H→L (99.2%)
CAM-B3LYP/6-311++G(d,p)	14.38	66.	1.393	1.425	1.465	13.94,	373 (0.57), H→L (94.6%)
//B3LYP/6-311++G(d,p)		7				15.82, 19.56	364 (0.85), H-1→L (94.7%)
M062X/6-311++G(d,p)	14.38	66.	1.393	1.425	1.465	13.94,	380 (0.69), H→L (95.8%)
//B3LYP/6-311++G(d,p)		7				16.07, 19.47	372 (0.83), H-1→L (95.7%)

^aSee Fig. 3 for geometrical parameters definitions; $\mu_g, \mu_{e1}, \mu_{e2}$ represent the dipole moments of the ground, first excited and second excited states, respectively.

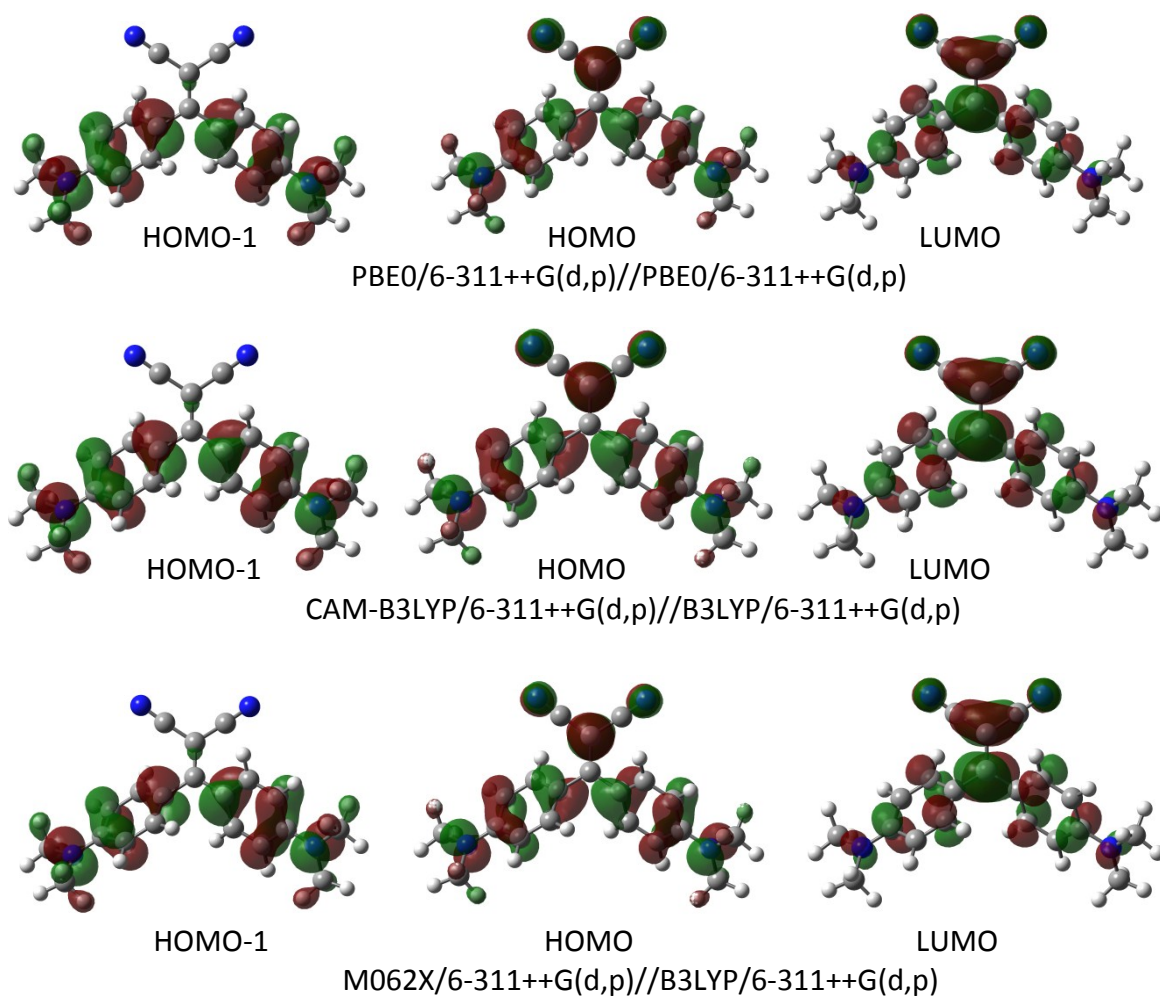


Fig. S3. Plots of HOMO-1 (left), HOMO (center) and LUMO (right) of the optimized geometry of **1** in toluene with isosurfaces value 0.03, as obtained by PBE0/6-311++G(d,p)//PBE0/6-311++G(d,p) (first line), CAM-B3LYP/6-311++G(d,p)//B3LYP/6-311++G(d,p) (second line) and M062X/6-311++G(d,p)//B3LYP/6-311++G(d,p) (third line) calculations.

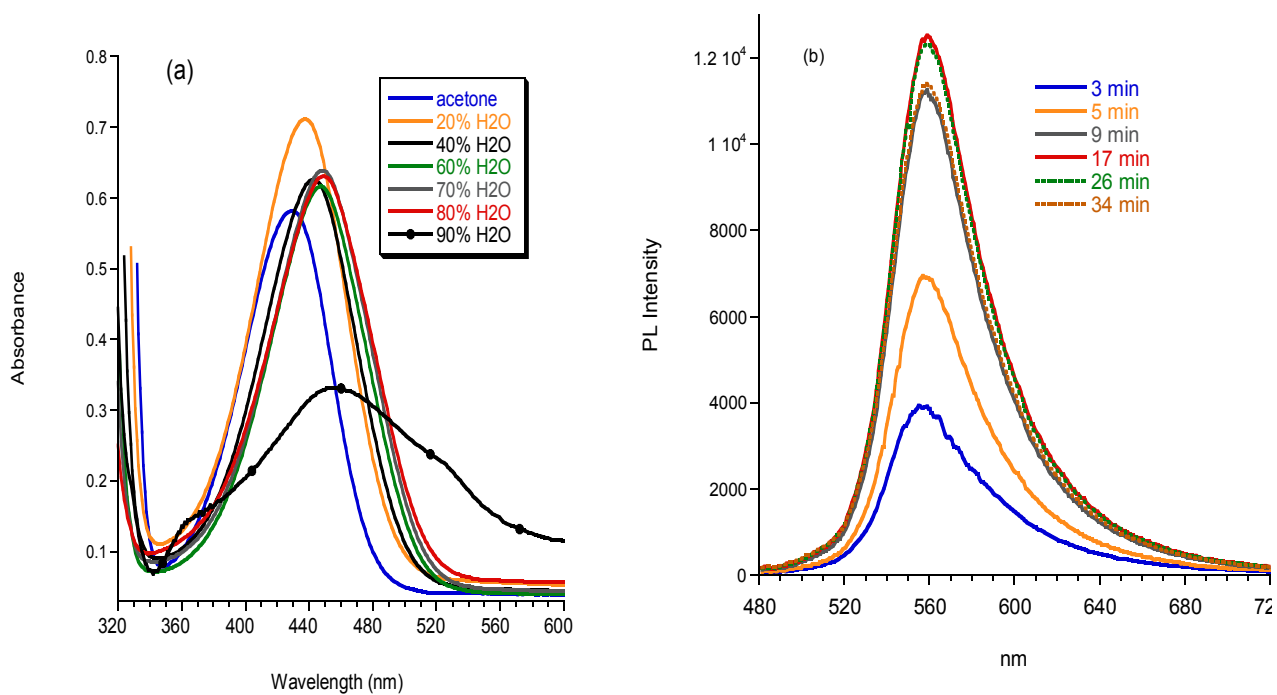


Fig. S4. (a) Optical absorption of **1** in acetone/H₂O mixtures, for different water fractions. (b) PL time evolution of the solution with 90% water fraction.

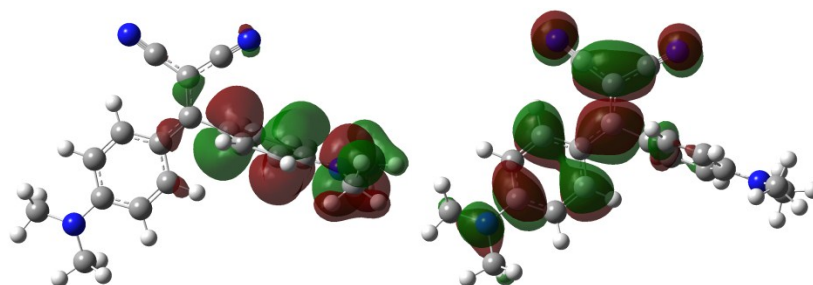


Fig. S5. Plots of HOMO (left) and LUMO (right) of the S₁ TD-PBE0/6-311++G(d,p) optimized geometry of **1** in toluene with isosurfaces value 0.02.

Table S2. Details of the Crystal Data and Structure Refinement for A - D.

	A	B	C	D
<i>Crystal Data</i>				
Empirical formula	C ₂₀ H ₂₀ N ₄	C ₂₀ H ₂₀ N ₄	C ₂₀ H ₂₀ N ₄	C ₂₁ H ₂₂ Cl ₂ N ₄
Moiety formula	C ₂₀ H ₂₀ N ₄	C ₂₀ H ₂₀ N ₄	C ₂₀ H ₂₀ N ₄	(C ₂₀ H ₂₀ N ₄)(CH ₂ Cl ₂)
Formula weight	316.40	316.40	316.40	401.33
Crystal system	Monoclinic	Monoclinic	Monoclinic	Monoclinic
Space group	<i>C2/c</i>	<i>C2/c</i>	<i>P2₁</i>	<i>P2₁/c</i>
<i>a</i> /Å	11.9266(11)	8.4920(7)	9.7959(12)	12.5444(8)
<i>b</i> /Å	9.3889(8)	13.9497(11)	9.9417(12)	22.3085(14)
<i>c</i> /Å	15.6279(14)	15.0750(14)	17.678(2)	7.5898(5)
β /Å	97.498(1)	100.062(1)	94.478(2)	105.350(1)
<i>V</i> /Å ³	1735.0(3)	1758.3(3)	1716.4(4)	2048.2(2)
<i>Z</i>	4	4	4	4
Temperature/K	293(2)	293(2)	150(2)	180(2)
Density (calc.) <i>D_x</i> /Mg m ⁻³	1.211	1.195	1.224	1.301
Absorption coeff. μ /mm ⁻¹	0.074	0.073	0.075	0.330
Color, habit	orange, prism	orange, rod	yellow, needle	yellow, plate
Dimensions /mm	0.30×0.20×0.12	0.50×0.16×0.14	0.40×0.06×0.06	0.34×0.22×0.02
<i>Data Collection</i>				
radiation, λ /Å	Mo K α , 0.71073			
$2\theta_{\max}$ /°	55.86	59.64	64.40	49.34
<i>h</i> range	-15→15	-11→11	-14→14	-13→13
<i>k</i> range	-12→12	-19→19	-14→14	-19→19
<i>l</i> range	-20→20	-21→21	-26→26	-26→26
Measured reflections	14369	16782	28874	55474
Independent reflections	2074	2531	11008	7102
Reflections with $I > 2\sigma(I)$	1498	1782	8262	6162
<i>R</i> _{int}	0.0249	0.0252	0.0368	0.0577
<i>Refinement on F²</i>				
Data, restraints, parameters	2074, 0, 112	2531, 0, 112	11008, 1, 433	7102, 1, 488
<i>S</i>	1.017	1.043	1.010	1.049
Final <i>R</i> , <i>wR</i> [$F^2 > 2\sigma(F^2)$]	0.0428, 0.1112	0.0462, 0.1265	0.0489, 0.0982	0.0377, 0.0920
Final <i>R</i> , <i>wR</i> (all data)	0.0620, 0.1242	0.0686, 0.1429	0.0788, 0.1096	0.0478, 0.0985
(Δ / σ) _{max}	0.001	0.001	0.001	0.001
$\Delta\rho_{\max}$, $\Delta\rho_{\min}$ /eÅ ⁻³	0.168, -0.154	0.176, -0.136	0.309, -0.214	0.359, -0.270

Detailed analysis of crystal packing of A-D.

In both **A** and **B** structures, molecules are arranged along chains connected through weak C–H \cdots N hydrogen bonds (for **A**: C11–H11B \cdots N1[i] with $d = 2.69\text{\AA}$, $\theta = 153.8^\circ$; for **B**: C9–H9 \cdots N1[i] with $d = 2.65\text{\AA}$, $\theta = 139.7^\circ$ and C11–H11B \cdots N1[ii], $d = 2.64\text{\AA}$, $\theta = 141.2^\circ$, d and θ being the H \cdots N distance and the C–H \cdots N angle, respectively, see Figs. S6-S8 for atom numbering).^{S1} In both structures, weak $\pi - \pi$ stacking interactions connect the chains each other (see Fig. 4). In structure of polymorph **C**, the two molecules of the a.u. are connected through multiple C–H \cdots π interactions involving the C4 \div C9 and C24 \div C29 phenyl rings in almost perpendicular configuration (the dihedral angle between them is $87.8(1)^\circ$), the shorter contact being C5–H5 \cdots C25 with $d = 2.81\text{\AA}$. Several C–H \cdots N and additional C–H \cdots π interactions contribute to stabilize the structure of **C**.^{S2} A dense intermolecular interactions network is as well observed for **D**, where molecules are arranged along pseudo-planes where they are connected through C10–H10B \cdots N3[i] (d , 2.52\AA ; θ , 175.0°) in one direction and C20–H20A \cdots N1[ii] (d , 2.60\AA ; θ , 145.3°) hydrogen bonds in the other direction. C–H \cdots N and C–H \cdots π interactions connect the planes each other (C5–H5 \cdots N1[iii], d , 2.70\AA , θ , 158.7° ; C11–H11A \cdots C7[iv], d , 2.80\AA , θ , 138.2° ; C17–H17 \cdots C16[v], d , 2.89\AA , θ , 141.8°).^{S1}

S1. Symmetry codes for the equivalent positions of **A**, [i]= $-x+3/2, -y+1/2, -z+1$; **B**, [i]= $-x+3/2, y-1/2, -z+3/2$, [ii]= $-x+1, -y+2, -z+1$; **C**, [i]= $-x, +y-1/2, -z+2$; [ii]= $-x+1, +y-1/2, -z+1$; [iii]= $x-1, +y, +z$; [iv]= $x-1, +y-1, +z$; [v]= $x, y+1, +z$; [vi]= $x, +y-1, +z$; [vii]= $-x, +y+1/2, -z+2$; **D**, [i]= $-x+2, y-1/2, -z+1/2$, [ii]= $x-1, y, z$, [iii]= $x, -y+3/2, z+1/2$, [iv]= $-x+2, -y+1, -z$, [v]= $x, -y+3/2, +z-1/2$. Only intermolecular contacts below the sum of van der Waals radii have been reported.

S2. C–H \cdots N contacts in **C** structure, from the shorter to the longer one: C30–H30A \cdots N5[i], d , 2.46\AA , θ , 151.9° ; C19–H19A \cdots N3[ii], d , 2.48\AA , θ , 167.2° ; C31–H31C \cdots N3[iii], d , 2.56\AA , θ , 177.2° ; C10–H10A \cdots N5[iv], d , 2.57\AA , θ , 139.5° ; C20–H20A \cdots N3[v], d , 2.58\AA , θ , 162.9° ; C35–H35 \cdots N4[vi], d , 2.62\AA , θ , 149.4° . Additional C–H \cdots π contacts in **C** structure, from the shorter to the longer one: C19–H19B \cdots C36[ii], d , 2.78\AA ; C11–H11C \cdots C12[iii], d , 2.82\AA ; C34–H34 \cdots C16[v], d , 2.84\AA ; C8–H8 \cdots C29[vi], d , 2.89\AA ; C30–H30C \cdots C6[vii], d , 2.90\AA . See note S1 for the symmetry codes.

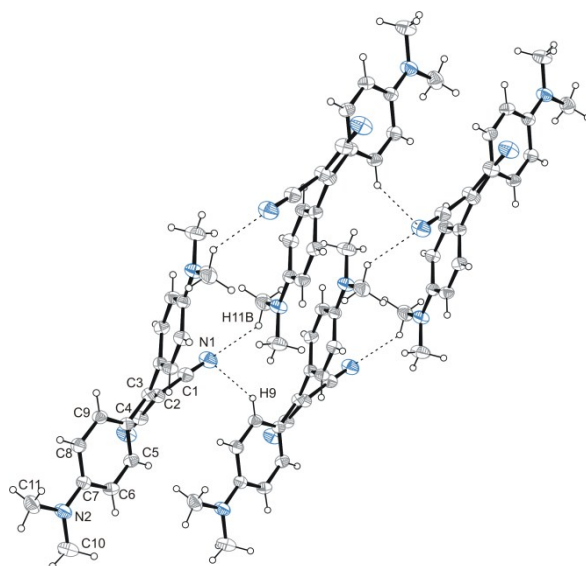


Fig. S6. Partial view of the crystal packing of **B**, where hydrogen bonds (short dashes) are included. Ellipsoids drawn at 30% probability level.

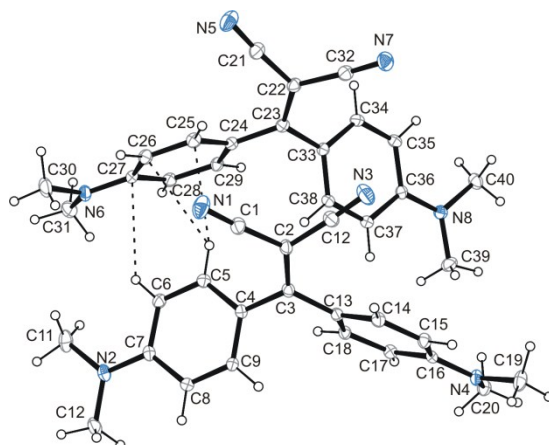


Fig. S7. Plot of the asymmetric unit of **C**, where hydrogen bonds (short dashes) are included. Ellipsoids drawn at 30% probability level.

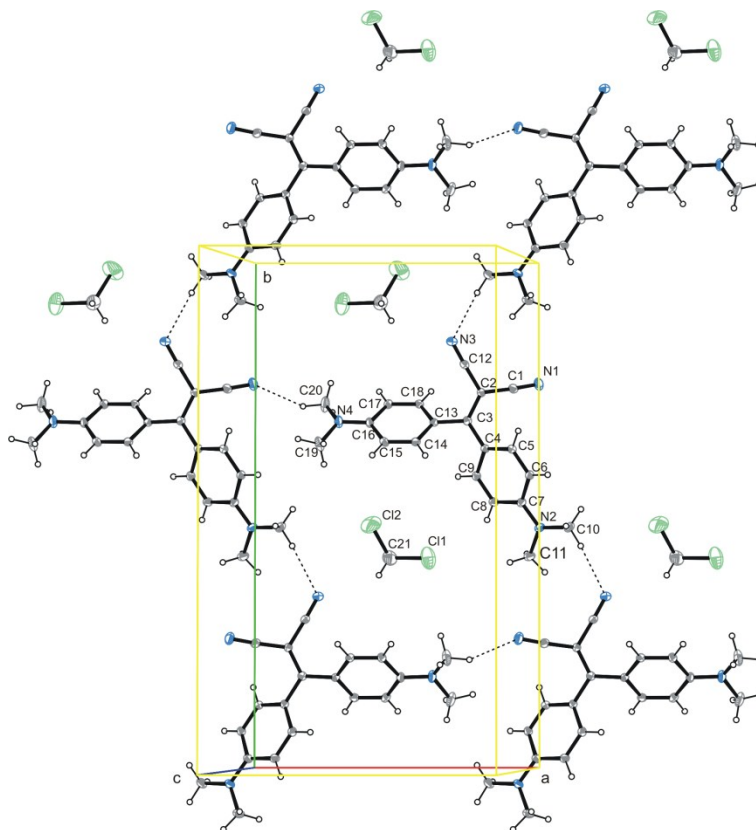


Fig. S8. Partial view of the crystal packing of **D** along the *c* axis, where selected hydrogen bonds (short dashes) are included. Ellipsoids drawn at 30% probability level.

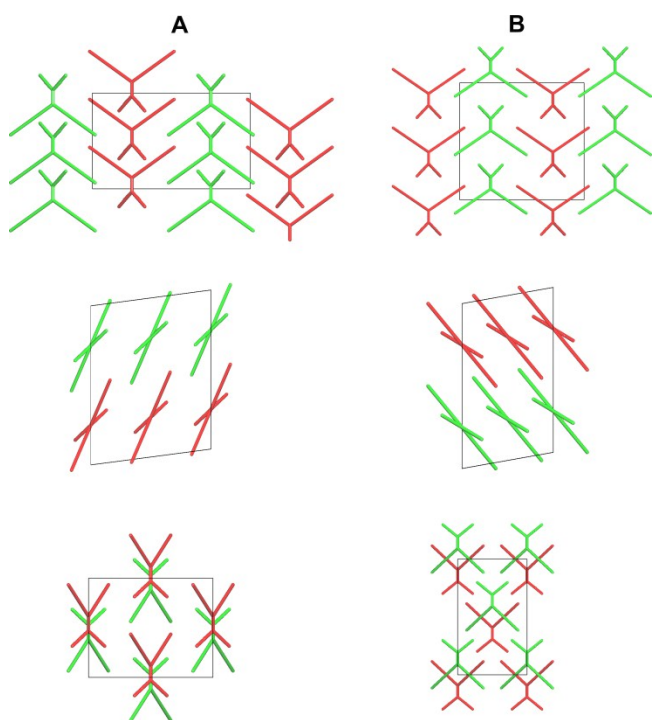


Fig. S9. Crystal packing in compounds **A** (left) and **B** (right). Views of the simplified molecules down the *a* (top), *b* (middle) and *c* (bottom) crystallographic directions in the two compounds.

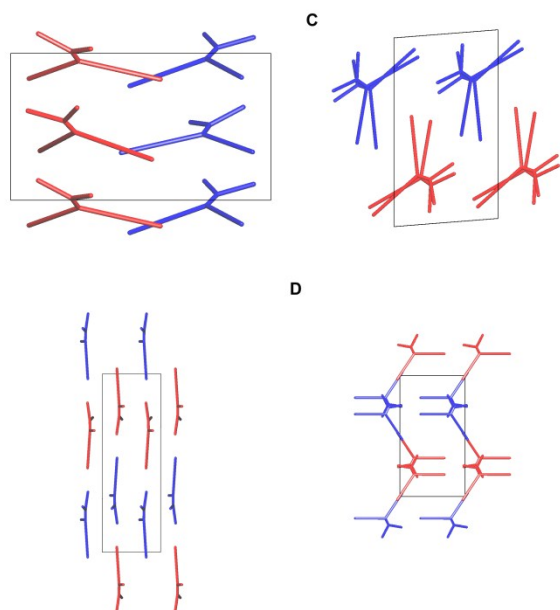


Fig. S10. Crystal packing in compounds **C** (top) and **D** (bottom). Views of the simplified molecules down the *a* (left) and *c* (right) crystallographic directions in the two compounds.

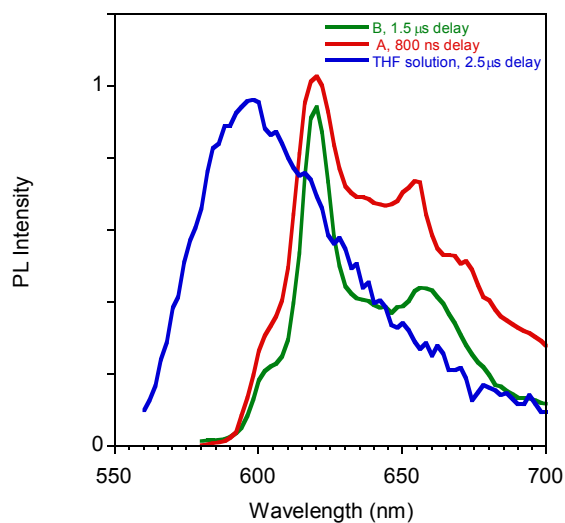


Fig. S11. Phosphorescence spectra measured at 77K.

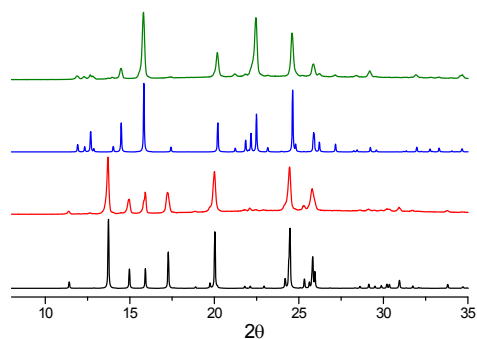


Fig. S12. XRPD patterns monitoring the quenching process for compound **A** and its transformation to **B**: simulated from crystal structure data of **A** (black); powders of **A** obtained by fast precipitation (red); simulated from crystal structure data of **B** (blue); microcrystalline powders obtained by melting at 260°C and subsequent quenching in liquid nitrogen of powders of **A**.

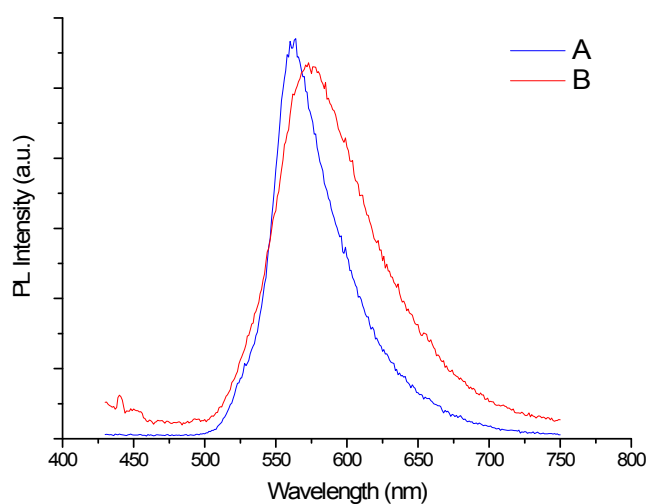


Fig. S13. PL spectra of powders of phase **A** (blue line) and phase **B** (red line) as obtained by melting and fast cooling of phase **A**.

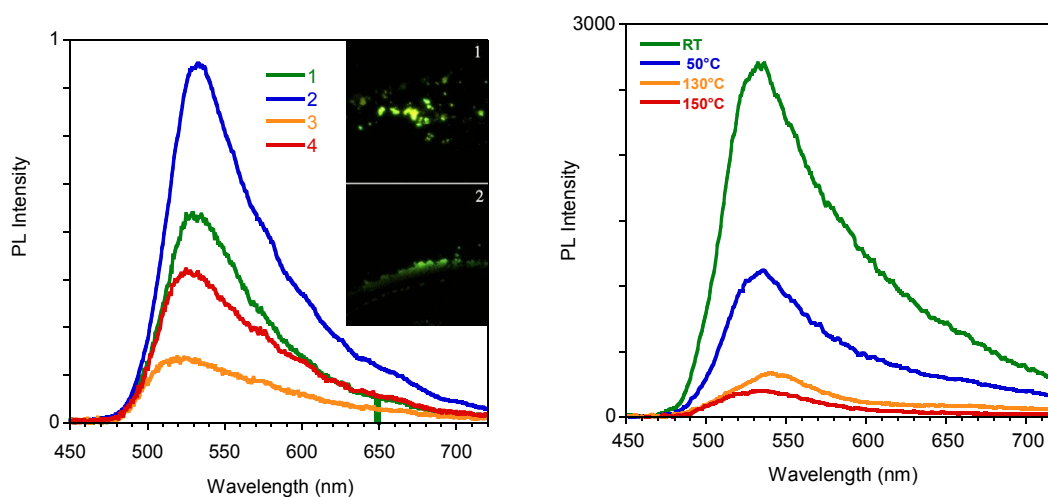
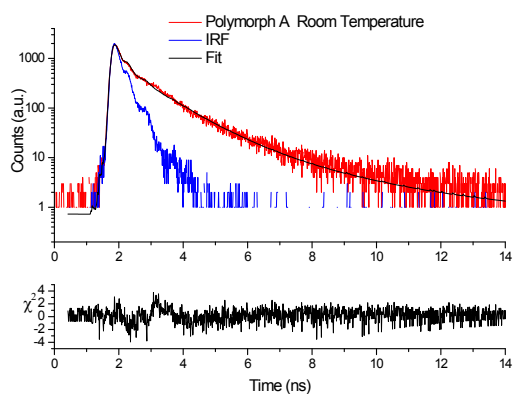


Fig. S14. Left: PL spectra of crystal **C** during grinding, in the inset two pictures taken during grinding. Right: PL spectra of crystal **C** during a heating cycle.

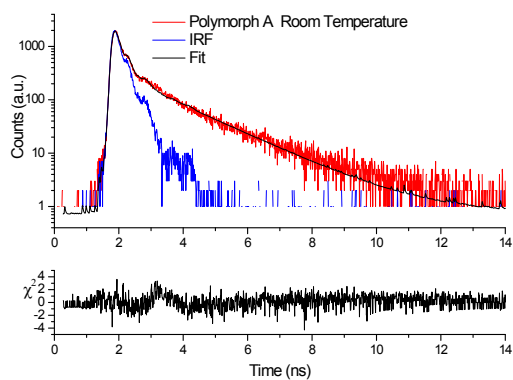
Time resolved analysis

Polymorph A, Room Temperature

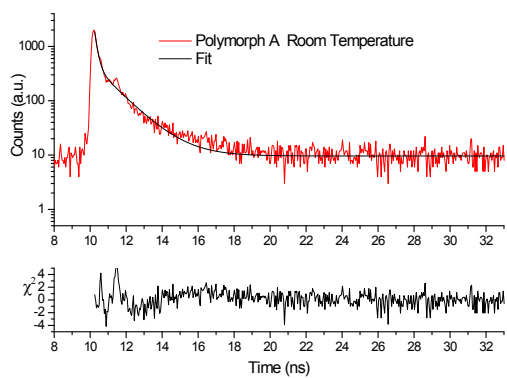
emission 530nm



emission 583nm



emission 620nm



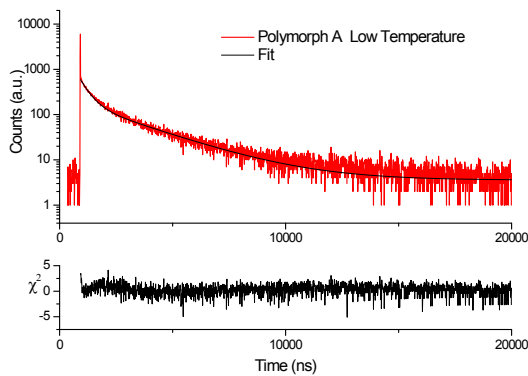
Decay fits parameters of Polymorph A, room temperature

emission	530nm	583nm	620nm
τ_1	34ps (48.5%)	23.17ps (63%)	0.15ns (35%)
τ_2	1.01ns (43%)	1.56ns (37%)	1.29ns (65%)
τ_3	2.81ns (8.5)	--	--
$\chi(2)$	1.17	1.063	1.57
τ_{av}	1.61 ns	1.52 ns	1.22 ns

the average lifetime τ_{av} is obtained as

$$\tau_{av} = \frac{\sum_i \tau_i^2 A_i}{\sum_i A_i \tau_i}$$

decay at 77K, 620nm.

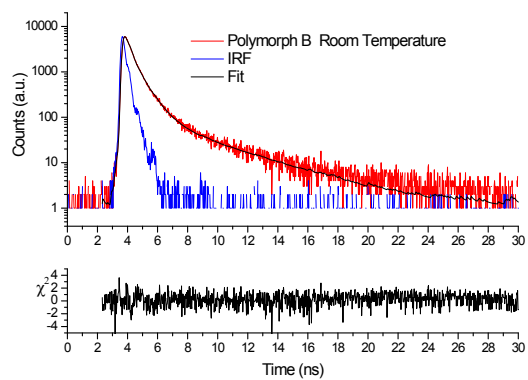


Decay fits parameters of Polymorph A, 77K

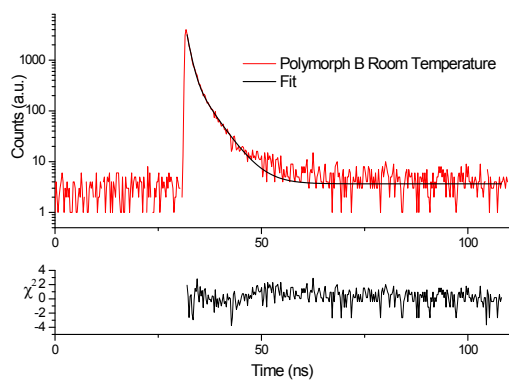
emission	620nm
τ_1	0.4 μ s (32.55%)
τ_2	2.5 μ s (67.45%)
$\chi(2)$	1.2
τ_{av}	1.82 μ s

Polymorph B, Room Temperature

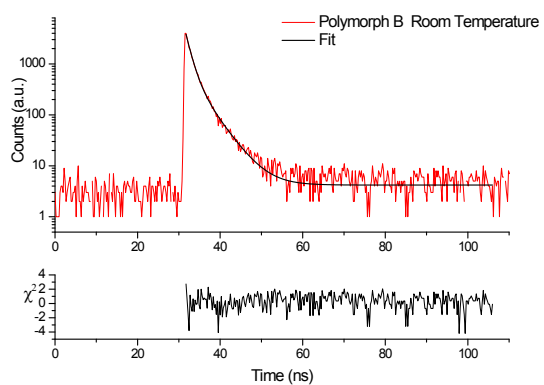
emission 553nm



emission 620 nm



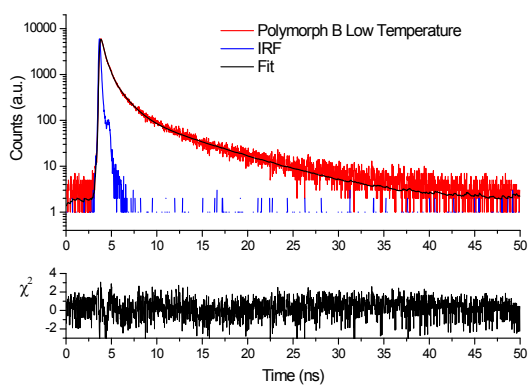
emission 650 nm



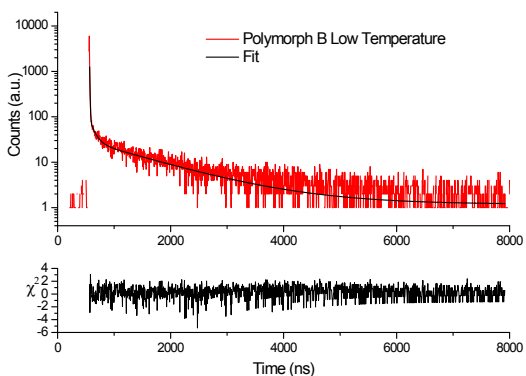
Decay fits parameters of Polymorph B, room temperature

emission	553nm	620nm	650nm
τ_1	0.18ns (50%)	0.90ns (60.75%)	1.25ns(62.10%)
τ_2	0.74ns (40.6%)	3.65ns (39.25%)	3.74ns(37.90%)
τ_3	3.89ns (9.4%)	--	--
$\chi(2)$	1.12	1.37	1.39
τ_{av}	2.20 ns	2.89ns	2.19ns

77K, emission 553nm:



77K, emission 620nm:

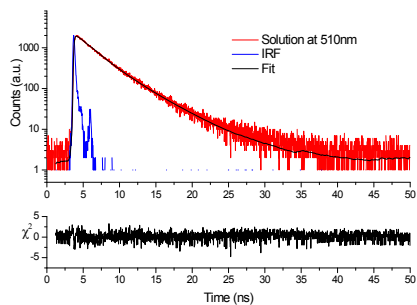


Decay fits parameters of Polymorph **B**, 77K

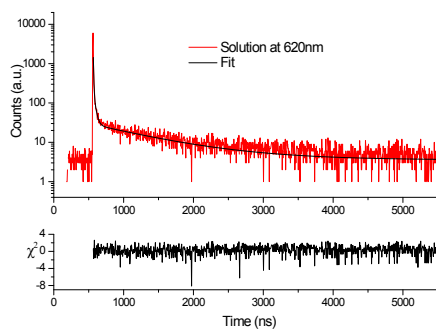
emission	553nm	620nm
τ_1	0.34ns (46.82%)	5.75ns (30%)
τ_2	1.34ns (34.92%)	87.09ns (10%)
τ_3	6.65ns (18.26%)	1.15 μ s (60%)
$\chi(2)$	1.15	1.05
τ_{av}	1.84 ns	1.13 μ s

THF solution at 77 K

emission 510nm:



emission 620nm:



emission	510nm	620nm
τ_1	2.0ns (47.78%)	4.72ns (35.92%)
τ_2	4.4ns (52.22%)	27.76ns (12.56%)
τ_3	--	0.93 μ s(51.52%)
$\chi(2)$	1.088	1.34
τ_{av}	3.70 ns	0.93 μ s